

Phenomenological description of the nonlocal magnetization relaxation in magnonics, spintronics, and domain-wall dynamics

Weiwei Wang,¹ Mykola Dvornik,^{2,3} Marc-Antonio Bisotti,¹ Dmitri Chernyshenko,¹ Marijan Beg,¹ Maximilian Albert,¹ Arne Vansteenkiste,² Bartel V. Waeyenberge,² Andriy N. Kuchko,^{4,5} Volodymyr V. Kruglyak,⁶ and Hans Fangohr¹

¹*Engineering and the Environment, University of Southampton, Southampton, United Kingdom*

²*DyNaMat Lab, Ghent University, Ghent, Belgium*

³*Physics Department, University of Gothenburg, 412 96 Gothenburg, Sweden*

⁴*Physical and Technical Department, Donetsk National University, Donetsk, Ukraine*

⁵*Institute of Magnetism, National Academy of Sciences of Ukraine, 36b Vernadskogo Avenue, Kiev, 03142, Ukraine*

⁶*School of Physics, University of Exeter, Exeter, United Kingdom*

(Received 3 March 2015; revised manuscript received 28 July 2015; published 21 August 2015)

A phenomenological equation called the Landau-Lifshitz-Baryakhtar (LLBar) [Zh. Eksp. Teor. Fiz **87**, 1501 (1984) [Sov. Phys. JETP **60**, 863 (1984)]] equation, which could be viewed as the combination of the Landau-Lifshitz (LL) equation and an extra “exchange-damping” term, was derived by Baryakhtar using Onsager’s relations. We interpret the origin of this exchange damping as nonlocal damping by linking it to the spin current pumping. The LLBar equation is investigated numerically and analytically for the spin-wave decay and domain-wall motion. Our results show that the lifetime and propagation length of short-wavelength magnons in the presence of nonlocal damping could be much smaller than those given by the LL equation. Furthermore, we find that both the domain-wall mobility and the Walker breakdown field are strongly influenced by the nonlocal damping.

DOI: [10.1103/PhysRevB.92.054430](https://doi.org/10.1103/PhysRevB.92.054430)

PACS number(s): 75.78.Cd, 76.50.+g, 75.60.Ch

I. INTRODUCTION

The genuine complexity of magnetic and spintronic phenomena occurring in magnetic samples and devices imposes both fundamental and technical limits on the applicability of quantum-mechanical and atomistic theories to their modeling. To a certain degree, this challenge can be circumvented by exploiting phenomenological theories based on the continuous-medium approximation. The theories operate with the magnetization (i.e., the magnetic moment density) and the effective magnetic field as generalized coordinates and forces, respectively [1,2]. The effective magnetic field is defined in terms of various magnetic material parameters, which are determined by fitting theoretical results to experimental data and, at least in principle, can be calculated using the quantum-mechanical or atomistic methods. However, solving the phenomenological models analytically is still a formidable task in the majority of practically important cases. The difficulty is primarily due to the presence of the long-range magnetodipole interaction and associated nonuniformity of the ground-state configurations of both the magnetization and effective magnetic fields. Hence, the phenomenological models are solved instead numerically, using either finite-difference or finite-element methods realized in a number of micromagnetic solvers [3–7].

Traditionally, the software for such numerical micromagnetic simulations of magnetization dynamics is based on solving the Landau-Lifshitz equation [1] with a transverse magnetic relaxation term, either in the original (Landau) [1] or “Gilbert” [8] form. Over time, dictated by the experimental and technological needs, the solvers have been modified to include finite-temperature effects [9] and additional contributions to the magnetic energy (and therefore to effective magnetic field) [10]. The recent advances in spintronics and magnonics have led to the implementation of various spin-transfer-torque terms [11,12] and periodic boundary conditions [13–15].

Furthermore, the progress in experimental investigations of ultrafast magnetization dynamics [16] has exposed the need to account for the variation of the length of the magnetization vector in response to excitation by femtosecond optical pulses, leading to inclusion of the longitudinal relaxation of the magnetization within the formalism of numerical micromagnetics [17]. Provided that good agreement between the simulated and measured results is achieved, a microscopic (i.e., quantum-mechanical or atomistic) interpretation of the experiments can then be developed.

The described strategy relies on the functional completeness of the phenomenological model. For instance, a forceful use of incomplete equations to describe phenomena originating from terms missing from the model may result in false predictions and erroneous values of fitted parameters and eventually in incorrect conclusions. The nature of the magnetic relaxation term and associated damping constants in the Landau-Lifshitz equation is of paramount importance both fundamentally and technically. It is this term that is responsible for establishment of equilibrium both within the magnetic subsystem and with its environment (e.g., electron and phonon subsystems), following perturbation by magnetic fields, spin currents, and/or optical pulses [16]. Moreover, it is the same term that will eventually determine the energy efficiency of any emerging nanomagnetic devices, including both those for data storage [18] and manipulation [19].

In this paper, we demonstrate how the phenomenological magnetic relaxation term derived by Baryakhtar to explain the discrepancy between magnetic damping constants obtained from ferromagnetic resonance (FMR) and magnetic domain-wall velocity measurements in dielectrics [20–22] can be applied to magnetic metallic samples. We show that the Landau-Lifshitz equation with the Baryakhtar relaxation term (the Landau-Lifshitz-Baryakhtar or, simply, LLBar equation) contains the Landau-Lifshitz-Gilbert (LLG) equation as a

special case while also naturally including the contribution from the nonlocal damping in the tensor form of Zhang and Zhang [23] and De Angeli *et al.* [24]. The effects of the longitudinal relaxation and the anisotropic transverse relaxation on the magnetization dynamics excited by optical and magnetic field pulses, respectively, in continuous films and magnetic elements were discussed, e.g., in Refs. [17,25,26]. So here we focus primarily on the manifestations of the Baryakhtar relaxation in problems specific to magnonics [19] and domain-wall dynamics [27,28]. This is achieved by incorporating the LLBar equation within the code of the Object Oriented Micromagnetic Framework (OOMMF) [3], probably the most popular micromagnetic solver currently available, and by comparing the results of simulations with those from simple analytical models. Specifically, we demonstrate that the Baryakhtar relaxation leads to increased damping of short-wavelength spin waves and to modification of the domain-wall mobility, with the latter also being affected by the longitudinal relaxation strength.

This paper is organized as follows. In Sec. II, we review and interpret the Baryakhtar relaxation term. In Sec. III, we calculate and analyze the spin-wave decay in a thin magnetic nanowire. In Sec. IV, we simulate the suppression of standing spin waves in thin film. In Sec. V, we analyze the domain-wall motion driven by the external field and compare the relative strength of contributions from the longitudinal and nonlocal dampings. We conclude the discussion in Sec. VI.

II. BASIC EQUATIONS

In the most general case, the LLBar equation can be written as [20,25]

$$\frac{\partial \mathbf{M}}{\partial t} = -\gamma \mathbf{M} \times \mathbf{H}_{\text{eff}} + \mathbf{R}, \quad (1)$$

where γ (>0) is the gyromagnetic ratio and the relaxation term \mathbf{R} is

$$\mathbf{R} = \hat{\Lambda}_r \cdot \mathbf{H}_{\text{eff}} - \hat{\Lambda}_{e,sp} \frac{\partial^2 \mathbf{H}_{\text{eff}}}{\partial x_s \partial x_p}. \quad (2)$$

Here and in the rest of the paper, the summation is automatically assumed for repeated indices. The two relaxation tensors $\hat{\Lambda}_r$ and $\hat{\Lambda}_e$ describe relativistic and exchange contributions, respectively, as originally introduced in Refs. [21,29].

To facilitate comparison with the Landau-Lifshitz-Bloch (LLB) equation as written in Ref. [30], the magnetic interaction energy of the sample is defined as

$$w = w_\mu + \frac{\mu_0 (M^2 - M_e^2)^2}{8\chi M_e^2}, \quad (3)$$

where M_e is the equilibrium magnitude of the magnetization vector at a given temperature and zero micromagnetic effective field, i.e., the effective field derived from the micromagnetic energy density w_μ , as used in standard simulations at constant temperature under the condition $|\mathbf{M}| = M_e = \text{const}$ (i.e., with only the transverse relaxation included). The second term on the right-hand side of Eq. (3) describes the energy density induced by the small deviations of the magnetization length from its equilibrium value M_e at the given temperature, i.e., $|M^2 - M_e^2| \ll M_e^2$, and χ is the longitudinal magnetic

susceptibility. Therefore, the associated effective magnetic field is

$$\mathbf{H}_{\text{eff}} = -\frac{1}{\mu_0} \frac{\delta w}{\delta \mathbf{M}} = \mathbf{H}_\mu + \frac{1}{2\chi} (1 - n^2) \mathbf{M}, \quad (4)$$

where $\mathbf{n} = \mathbf{M}/M_e$ and \mathbf{H}_μ is the effective magnetic field associated with w_μ . Hereafter we assume that our system is in contact with the heat bath, so that the equilibrium temperature and associated values of M_e and χ remain constant irrespective of the magnetization dynamics.

In accordance with the standard practice of both micromagnetic simulations and analytical calculations, to solve LLBar equations (1)–(4), one first needs the corresponding static equations obtained by setting the time derivatives to zero and thereby to derive the spatial distribution of the magnetization in terms of both its length and direction. We note that, in general (e.g., as in the case of a domain wall), the resulting distribution of the longitudinal effective field and therefore also of the equilibrium magnetization length is nonuniform, so that the length is not generally equal to M_e . With the static solution at hand, the dynamical problem is solved to find the temporal evolution of the magnetization length and direction following some sort of a perturbation. Crudely speaking, the effect of the relaxation terms is that, at each moment of time, the magnetization direction relaxes towards the instantaneous direction of the effective magnetic field, while the magnetization length relaxes towards the value prescribed by the instantaneous longitudinal effective magnetic field. The effective field itself varies with time, which makes the problem rather complex. However, this is the same kind of complexity as the one that has always been inherent in micromagnetics. Accounting for the longitudinal susceptibility within the LLBar equation only brings another degree of freedom (the length of the magnetization) into the discussion. One should note, however, that the longitudinal susceptibility has a rather small value at low temperature, so its account is only required at temperatures of the order of the Curie temperature.

We neglect throughout the paper any effects due to the anisotropy of relaxation, which could be associated with, e.g., the crystalline structure of the magnetic material [20,25]. This approximation is justified for polycrystalline and amorphous soft magnetic metals, as has been confirmed by simulations presented in Ref. [25]. Hence, we represent the relaxation tensors as $\hat{\Lambda}_r = \lambda_r \hat{I}$ and $\hat{\Lambda}_e = \lambda_e \hat{I}$, where parameters λ_r and λ_e are the relativistic and exchange relaxation damping constants and \hat{I} is the unit tensor. Then, Eq. (1) is reduced to

$$\partial_t \mathbf{M} = -\gamma \mathbf{M} \times \mathbf{H}_{\text{eff}} + \lambda_r \mathbf{H}_{\text{eff}} - \lambda_e \nabla^2 \mathbf{H}_{\text{eff}}. \quad (5)$$

We separate the equations describing the dynamics and relaxation of the length and direction of the magnetization vector. Representing the latter as a product of its magnitude and directional unit vector $\mathbf{M} = M \mathbf{m}$, we can write

$$M \frac{\partial \mathbf{m}}{\partial t} + \mathbf{m} \frac{\partial M}{\partial t} = -\gamma \mathbf{M} \times \mathbf{H}_{\text{eff}} + \mathbf{R}. \quad (6)$$

We multiply this equation by \mathbf{m} to obtain

$$\frac{\partial M}{\partial t} = \mathbf{m} \cdot \mathbf{R}. \quad (7)$$

Then, subtracting the product of Eq. (7) and \mathbf{m} from Eq. (6), we obtain

$$\frac{\partial \mathbf{m}}{\partial t} = -\gamma \mathbf{m} \times \mathbf{H}_{\text{eff}} + \frac{1}{M} \mathbf{R}_{\perp}, \quad (8)$$

where $\mathbf{R}_{\perp} = -\mathbf{m} \times (\mathbf{m} \times \mathbf{R})$. In the rest of the paper, we will use $\mathbf{A}_{\perp} \equiv (\mathbf{A})_{\perp} \equiv \mathbf{A} - (\mathbf{A} \cdot \mathbf{m})\mathbf{m}$ to represent the component of vector \mathbf{A} that is perpendicular (transverse) to vector \mathbf{m} . Note that only the perpendicular component of the torque contributes to $\partial_t \mathbf{m} \equiv \partial \mathbf{m} / \partial t$. For given temperature, M_e is constant, and we can define $\alpha = \lambda_r / (\gamma M_e)$. In the limiting case of $\chi \rightarrow 0$, $M \rightarrow M_e$, and thus, α is recognized as the Gilbert damping constant from the LLG equation. Let us now consider the case of $\hat{\Lambda}_e \neq 0$. The corresponding contribution to the relaxation term, which we denote here as \mathbf{B}_{Bar} , can be written as

$$\mathbf{B}_{\text{Bar}} = -\lambda_e \nabla^2 \mathbf{H}_{\text{eff}} \equiv -\partial_i \mathbf{j}_i, \quad (9)$$

where $\partial_i \equiv \partial / \partial x_i$ and the quantity $\mathbf{j}_i = -\lambda_e \partial_i \mathbf{H}_{\text{eff}}$ has the form of some magnetization current density (magnetization flux).

For the following, it is useful to split the effective field into its perpendicular (relative to \mathbf{m}) part ($\mathbf{H}_{\text{eff}}^{\perp}$, “perpendicular field”) and parallel part ($\mathbf{H}_{\text{eff}}^{\parallel}$, “parallel field”), i.e., $\mathbf{H}_{\text{eff}} = \mathbf{H}_{\text{eff}}^{\perp} + \mathbf{H}_{\text{eff}}^{\parallel}$, and then to consider the associated magnetic fluxes and torques separately. The magnetic flux of $\mathbf{j}_{\parallel,i} = -\lambda_e \partial_i \mathbf{H}_{\text{eff}}^{\parallel}$, and then the contribution of the associated torque $\boldsymbol{\tau}_{\parallel} = -\partial_i \mathbf{j}_{\parallel,i}$ onto \mathbf{m} is

$$(\boldsymbol{\tau}_{\parallel})_{\perp} = -2\lambda_e \partial_i \mathbf{H}_{\text{eff}}^{\parallel} \partial_i \mathbf{m} - \lambda_e \mathbf{H}_{\text{eff}}^{\parallel} (\nabla^2 \mathbf{m})_{\perp}. \quad (10)$$

The perpendicular field can be represented as

$$\mathbf{H}_{\text{eff}}^{\perp} = \frac{1}{\gamma M^2} \left[\mathbf{M} \times \frac{\partial \mathbf{M}}{\partial t} \right] + O(\mathbf{R}) \approx \frac{1}{\gamma} [\mathbf{m} \times \partial_t \mathbf{m}]. \quad (11)$$

So we can write for the magnetization flux associated with the perpendicular field

$$\mathbf{j}_{\perp,i} = -(\lambda_e / \gamma) \partial_i (\mathbf{m} \times \partial_t \mathbf{m}). \quad (12)$$

The right-hand side of Eq. (12) could be regarded as the torque generated by spin current pumping since $\mathbf{m} \times \partial_t \mathbf{m}$ can be considered the exchange spin current [31], and then for the associated perpendicular torque $\boldsymbol{\tau}_{\perp}$, we obtain

$$\boldsymbol{\tau}_{\perp} = -\partial_i \mathbf{j}_{\perp,i} = -\sigma M_e \partial_i \partial_t (\mathbf{m} \times \partial_t \mathbf{m}), \quad (13)$$

where we have introduced the variable $\sigma = \lambda_e / (\gamma M_e)$. We show that the torque $(\boldsymbol{\tau}_{\perp})_{\perp}$ could be written as (see Appendix A for details)

$$(\boldsymbol{\tau}_{\perp})_{\perp} = M_e [\mathbf{m} \times (\mathcal{D} \cdot \partial_t \mathbf{m}) - \sigma \mathbf{m} \times \nabla^2 \partial_t \mathbf{m}], \quad (14)$$

where \mathcal{D} is a 3×3 tensor [23,32],

$$\mathcal{D}_{\alpha\beta} = 2\sigma (\mathbf{m} \times \partial_i \mathbf{m})_{\alpha} (\mathbf{m} \times \partial_i \mathbf{m})_{\beta} - \sigma (\partial_i \mathbf{m} \cdot \partial_i \mathbf{m}) \delta_{\alpha\beta}. \quad (15)$$

In the limit of $\chi \rightarrow 0$, we assume $\mathbf{H}_{\text{eff}}^{\parallel} = 0$ and therefore obtain

$$\begin{aligned} \partial_t \mathbf{m} &= -\gamma \mathbf{m} \times \mathbf{H}_{\text{eff}} - \gamma \alpha \mathbf{m} \times (\mathbf{m} \times \mathbf{H}_{\text{eff}}) \\ &\quad + \mathbf{m} \times (\mathcal{D} \cdot \partial_t \mathbf{m}) - \sigma \mathbf{m} \times \nabla^2 \partial_t \mathbf{m}. \end{aligned} \quad (16)$$

At the same time, Eq. (8) can then be written as

$$\frac{\partial \mathbf{m}}{\partial t} = -\gamma \mathbf{m} \times \mathbf{H}_{\text{eff}} - \gamma \mathbf{m} \times (\mathbf{m} \times \mathbf{H}_{\text{eff}}^{\text{B}}), \quad (17)$$

where

$$\mathbf{H}_{\text{eff}}^{\text{B}} = \alpha \mathbf{H}_{\text{eff}} - \sigma \nabla^2 \mathbf{H}_{\text{eff}}^{\perp} \quad (18)$$

and $\mathbf{H}_{\text{eff}}^{\perp}$ is the transverse component of the effective field. The first term in Eq. (18) is kept as \mathbf{H}_{eff} since $\mathbf{m} \times \mathbf{H}_{\text{eff}} = \mathbf{m} \times \mathbf{H}_{\text{eff}}^{\perp}$. In practice, we use the simplified LLBar (sLLBar) Eq. (17) rather than Eq. (16) for numerical implementation. As shown in Eq. (16), the damping terms contain both the form $-\mathbf{m} \times \nabla^2 \partial_t \mathbf{m}$ [31,33] and tensor form $\mathbf{m} \times (\mathcal{D} \cdot \partial_t \mathbf{m})$ [23]. Hence, we conclude that the exchange damping can be explained as the nonlocal damping, and Eq. (17) is the phenomenological equation to describe the nonlocal damping.

The intrinsic Gilbert damping is generally considered to have a relativistic origin [1,34]. Phenomenologically, the Gilbert damping is local, and the damping due to the nonuniform magnetization dynamics is ignored [8]. The exchange relaxation term in the LLBar equation describes the nonlocal damping due to the nonuniform effective field. Despite the complexity of various damping mechanisms, the spin current \mathbf{j} in conducting ferromagnets can be calculated, e.g., using the time-dependent Pauli equation within the $s-d$ model. The spin current is then given by $\mathbf{j}_i = (g\mu_B \hbar G_0 / 4e^2) (\partial_t \mathbf{m} \times \partial_i \mathbf{m})$, where G_0 is the conductivity [23], and thus, the nonlocal damping of the tensor form can be obtained [23,32]. As we can see from Appendix A, these spin current densities \mathbf{j}_i and \mathbf{j}_i^{α} have the same form, and therefore, we can establish that $\sigma \sim g\mu_B \hbar G_0 / 4e^2 M_e$. The spin current component \mathbf{j}_i^{β} (see Appendix A) gives the term $-\mathbf{m} \times \nabla^2 \partial_t \mathbf{m}$ [31], and the value of σ can therefore be interpreted as $\sigma \sim (\gamma / \mu_0 M_e) (\hbar / 2)^2 n_e \tau_{\text{sc}} / m^*$, where n_e is the conduction electron density, m^* is the effective mass, and τ_{sc} is the transverse spin scattering time [35].

It is of interest to compare Eq. (5) with the LLB equation [30], which could be written as

$$\frac{\partial \mathbf{n}}{\partial t} = -\gamma \mathbf{n} \times \mathbf{H}_{\text{eff}} + \frac{\gamma \alpha_{\parallel}}{n^2} [\mathbf{n} \cdot \mathbf{H}_{\text{eff}}] \mathbf{n} - \frac{\gamma \alpha_{\perp}}{n^2} \mathbf{n} \times (\mathbf{n} \times \mathbf{H}_{\text{eff}}), \quad (19)$$

where $\mathbf{n} = \mathbf{M} / M_e(T)$ is the reduced magnetization and $M_e(T)$ is the equilibrium magnetization value at temperature T . The effective field \mathbf{H}_{eff} contains the usual micromagnetic contributions \mathbf{H}_{int} as well as the contribution from the temperature,

$$\mathbf{H}_{\text{eff}} = \mathbf{H}_{\text{int}} + \frac{m_e}{2\tilde{\chi}_{\parallel}} (1 - n^2) \mathbf{n}, \quad (20)$$

where $m_e = M_e(T) / M_e(0)$ and $\tilde{\chi}_{\parallel} = \partial m / \partial H$, with $m = M / M_e(0)$ [30]. By substituting Eq. (20) into Eq. (19), one arrives at

$$\begin{aligned} \frac{\partial \mathbf{n}}{\partial t} &= -\gamma \mathbf{n} \times \mathbf{H}_{\text{int}} + \gamma \alpha_{\parallel} (\mathbf{H}_{\text{int}})_{\parallel} + \gamma \alpha_{\perp} (\mathbf{H}_{\text{int}})_{\perp} \\ &\quad + \frac{\alpha_{\parallel} \gamma m_e}{2\tilde{\chi}_{\parallel}} (1 - n^2) \mathbf{n}. \end{aligned} \quad (21)$$

Meanwhile, if we neglect the λ_e term in Eq. (5) and insert the effective field equation (3) into Eq. (5), we obtain

$$\frac{\partial \mathbf{n}}{\partial t} = -\gamma \mathbf{n} \times \mathbf{H}_{\text{int}} + \gamma \lambda_r \mathbf{H}_{\text{int}} + \frac{\lambda_r \gamma}{2\chi} (1 - n^2) \mathbf{n}. \quad (22)$$

As we can see, Eq. (22) is a special case of the LLB equation with the assumption that $\alpha_{\perp} = \alpha_{\parallel} = \lambda_r / (\gamma M_e)$ and

$\chi = M_e(0)\tilde{\chi}_{\parallel}$. However, the LLB equation does not contain the λ_e term (nonlocal damping term), which is the main focus in this work.

III. SPIN-WAVE DECAY

To perform the micromagnetic simulation for the spin-wave decay, we have implemented Eq. (17) as an extension of the finite-difference micromagnetics package OOMMF. A new variable β for the exchange damping is introduced with $\sigma = \beta G$, where G is a coefficient to scale β to the same order as α . In practice, G was chosen to be $G = A/(\mu_0 M_e^2)$.

The simulation geometry has dimensions $L_x = 2002$ nm, $L_y = 2$ nm, and $L_z = 2$ nm, and the cell size is $1 \times 2 \times 2$ nm³. The magnetization aligns along the \mathbf{e}_x direction for the equilibrium state, and the parameters are typical of permalloy: the exchange constant $A = 1.3 \times 10^{-11}$ J/m, the saturation magnetization $M_e = 8.6 \times 10^5$ A/m, and the Gilbert damping coefficient $\alpha = 0.01$. The spin waves are excited locally in the region $0 \leq x \leq 2$ nm, and to prevent the spin-wave reflection the damping coefficient is increased linearly [36] from 0.01 at $x = 1802$ nm to 0.5 at $x = 2002$ nm.

Figure 1 illustrates the spin-wave-amplitude decay along the rod. The y component of magnetization unit vector m_y data for $30 \leq x \leq 1800$ nm was fitted using (23) to extract the wave vector k and the decay constant λ , and good agreement is observed due to the effective absence of spin-wave reflection. We use data after having computed the time development of the magnetization for 4 ns to reach a steady state. The injected spin-wave energy is absorbed efficiently enough within the right 200 nm of the rod due to the increased damping.

To analyze the simulation data, we exploit the uniform plane-wave assumption with its exponential amplitude decay due to energy dissipation, i.e., magnetization with the form $e^{i(kx - \omega t)} e^{-\lambda x}$, where λ is the characteristic parameter of the spin-wave damping. For a small-amplitude spin-wave propagation we have [37]

$$\mathbf{m} = \mathbf{e}_x + \mathbf{m}_0 e^{i(kx - \omega t)} e^{-\lambda x}, \quad (23)$$

where $|\mathbf{m}_0| \ll 1$, and the effective field of the long rod can be expressed as

$$\mathbf{H}_{\text{eff}} = H_s m_x \mathbf{e}_x + D \nabla^2 \mathbf{m}, \quad (24)$$

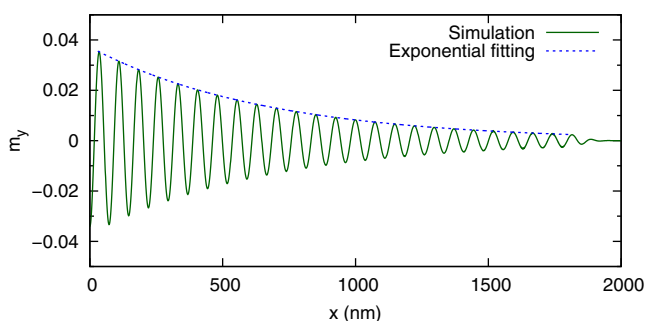


FIG. 1. (Color online) The spin-wave-amplitude decay along the rod, for a spin wave excited locally by applying a microwave $\mathbf{H} = H_0 \sin(2\pi f t) \mathbf{e}_y$, of frequency $f = 30$ GHz and amplitude $H_0 = 1000$ Oe in the region $0 \leq x \leq 2$ nm. The data were fitted using Eq. (23) with $\beta = 0.02$ and $\alpha = 0.01$.

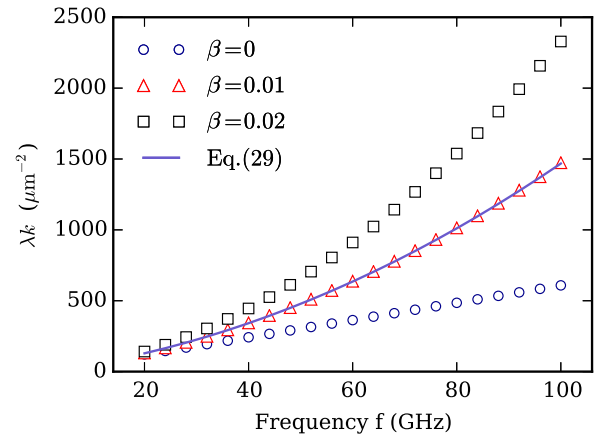


FIG. 2. (Color online) The spin-wave-decay constant–wave vector product λk as a function of the frequency for different β values. The slate blue line was drawn using Eq. (29) for the case $\beta = 0.01$.

where the “easy-axis” anisotropy field $H_s m_x \mathbf{e}_x$ originates from the demagnetizing field and the constant D measures the strength of the exchange field,

$$H_s = \frac{2K}{\mu_0 M_e} = \frac{1}{2} M_e, \quad D = \frac{2A}{\mu_0 M_e}. \quad (25)$$

To test the spin-wave decay for this system, a sinusoidal field $\mathbf{H} = H_0 \sin(2\pi f t) \mathbf{e}_y$ was applied to the rod in the region $0 \leq x \leq 2$ nm to generate spin waves.

Figure 2 shows the product of the spin-wave-decay constant λ and wave vector k as a function of the frequency. The dependence is linear for the $\beta = 0$ case, which is in agreement with the case with zero adiabatic spin torque [37]. The addition of a nonzero β term leads to a nonlinear relation and an amplitude of the spin-wave-decay constant that is significantly larger than that given by the linear dependence. We also performed the simulation for the $\chi > 0$ case by using Eq. (5), which shows that the β term is the leading factor for this nonlinearity (the relative error is less than 1% for $\chi = 1 \times 10^{-3}$). To analyze the nonlinear dependence, we introduce the complex wave vector \tilde{k} ,

$$\tilde{k} = k + \lambda i. \quad (26)$$

By linearizing Eq. (17) and setting the determinant of the matrix to zero, we obtained (see Appendix B for details)

$$(\omega + \tilde{\omega}_0 + i\tilde{\omega}_1)(\omega - \tilde{\omega}_0 + i\tilde{\omega}_1) = 0, \quad (27)$$

where $\tilde{\omega}_0 = \gamma(H_s + D\tilde{k}^2)$ and $\tilde{\omega}_1 = \alpha\tilde{\omega}_0 + \beta G\tilde{k}^2\tilde{\omega}_0$. The second term in Eq. (27) is expected to be equal to zero, i.e., $\tilde{\omega}_1 - i\omega + i\tilde{\omega}_0 = 0$. There are two scenarios to consider: The first is the $\beta = 0$ case, in which $k\lambda$ could be extracted by taking the imaginary part of \tilde{k}^2 in Eq. (26):

$$k\lambda = \frac{1}{2} \text{Im}\{\tilde{k}^2\} = \frac{\alpha\omega}{2(1 + \alpha^2)\gamma D}. \quad (28)$$

The linear dependence of $k\lambda$ as a function of frequency matches the data plotted in Fig. 2. For the $\beta > 0$ case, solving Eq. (27) for \tilde{k}^2 and using a linear approximation with respect

to the nonlocal damping constant β yields,

$$k\lambda \approx \frac{\omega}{2\gamma D}(\alpha + \beta Gk^2), \quad (29)$$

where the dispersion relation for the rod is $\omega = \gamma(H_s + Dk^2)$. Equation (29) shows there is an extra k^2 term associated with the exchange-damping term in addition to the linear dependence between $k\lambda$ and ω . The slate blue line in Fig. 2 is plotted using Eq. (29) with $\beta = 0.01$ and $\alpha = 0.01$, which shows a good approximation for the simulation data. In addition, this exchange damping could be important in determining the nonadiabatic spin torque. We could establish the value of β using the existing experimental data; for example, the transverse spin current data [35] give $\beta \sim 0.1$, which hints that the lifetime and propagation length of short-wavelength magnons could be much shorter than those given by the LLG equation [38].

IV. SUPPRESSION OF STANDING SPIN WAVES

In the presence of nonlocal damping, the high-frequency standing spin waves in the thin films are suppressed [38]. If the magnetization at the surfaces are pinned, the spin-wave resonance can be excited by a uniform alternating magnetic field [39]. With given out-of-plane external field H_z in the z direction, the frequencies of the excited spin waves of the film are given by [40]

$$\omega_n = \omega_0 + \omega_M \lambda_{\text{ex}}^2 \left(\frac{n\pi}{d}\right)^2, \quad (30)$$

where d is the film thickness, $\omega_0 = \gamma(H_z - M_e)$, $\omega_M = \gamma M_e$, and $\lambda_{\text{ex}} = \sqrt{2A/(\mu_0 M_e^2)}$. The excited spin-wave modes are labeled by the integer n , and an odd n has a nonvanishing interaction with the given uniform alternating magnetic field [39].

To reduce the simulation time, we consider a system with cross-sectional area $4 \times 4 \text{ nm}^2$ in the xy plane and apply the two-dimensional periodic boundary conditions [14] to the system. We use permalloy as the simulation material with external field $H_z = 1 \times 10^6 \text{ A/m}$, and the cell size is $4 \times 4 \times 2 \text{ nm}^3$. Instead of applying microwaves to the system, we calculate the magnetic absorption spectrum of the film by applying a sinc-function field pulse $h = h_0 \text{sinc}(\omega_0 t)$ to the system [41]. With the collected average magnetization data, the dynamic susceptibility χ is computed using Fourier transformation [42]. For example, the component χ_{yy} is computed using m_y when the pulse is parallel to the y axis.

Figure 3(a) shows the imaginary part of the dynamic susceptibility χ_{yy} for a film with $d = 300 \text{ nm}$. As we can see, the spin wave of modes $n = 1, 3, 5, \dots$ are excited, and the influence of the ‘‘exchange damping’’ is small. However, the presence of the exchange damping suppresses the spin-wave excitation ($n > 1$ mode) significantly for the film with thickness $d = 60 \text{ nm}$, as shown in Fig. 3(b). The reason is because the damping of the standing spin waves is proportional to k^4 in the presence of exchange damping [38].

V. DOMAIN-WALL MOTION

We implemented Eq. (5) in a finite-element-based micro-magnetic framework to study the effect of a parallel relaxation

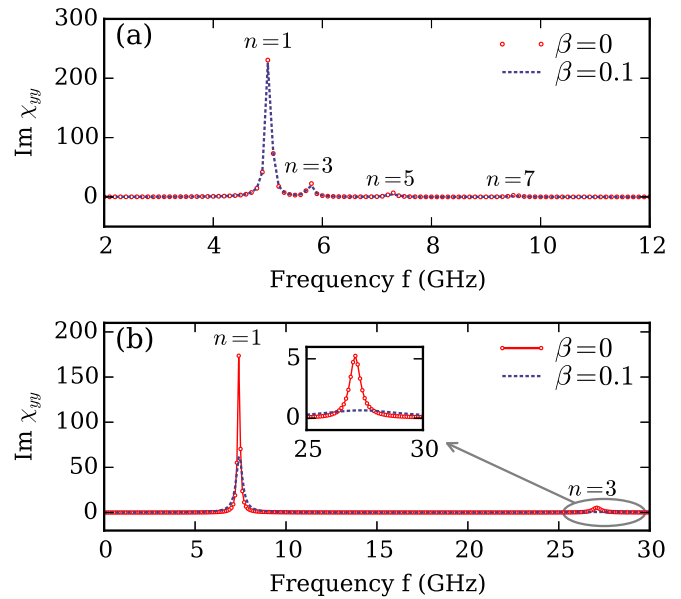


FIG. 3. (Color online) Imaginary parts of the dynamical susceptibility χ_{yy} of the film for (a) thickness $d = 300 \text{ nm}$ and (b) thickness $d = 60 \text{ nm}$.

process on domain-wall motion. The simulated system for the domain-wall motion is a one-dimensional (1D) mesh with a length of $20\,000 \text{ nm}$ and a discretization size of 4 nm ; a head-to-head domain wall is initialized with its center near $x = 500 \text{ nm}$. In this section, the demagnetizing fields are simplified as $\mathbf{H}_d = -N\mathbf{M}$, and the demagnetizing factors are chosen to be $N_x = 0$, $N_y = 0.2$, and $N_z = 0.8$, respectively. The domain wall moves under the applied field for 50 ns , and the domain-wall velocities at different external field strengths are computed. Figure 4 shows the simulation results of domain-wall motion under external fields for different susceptibilities without consideration of exchange damping, i.e., $\beta = 0$. For nickel and permalloy, the longitudinal susceptibility is around 10^{-4} at room temperature and increases with the temperature up to the Curie point [30]. We find that the longitudinal

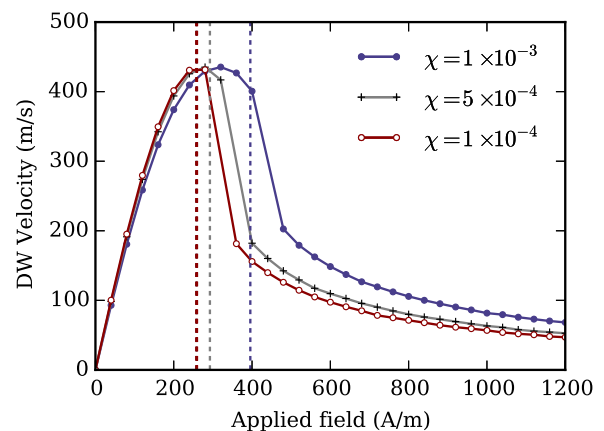


FIG. 4. (Color online) Simulation results of domain-wall velocities for various susceptibilities. The parameters used are $\alpha = 0.001$, $\beta = 0$, $N_y = 0.2$, and $N_z = 0.8$. The vertical dashed lines are the breakdown fields computed using Eq. (53).

susceptibilities have no influence on the maximum velocity but change the Walker breakdown field H_w significantly. The domain-wall velocity in the limit $\chi \rightarrow 0$ is almost the same as in the case of $\chi = 10^{-4}$, which could be explained by the difference proportional to the ratio of $(\chi/\alpha)^2$ in Eq. (53).

To investigate the effect of longitudinal magnetic susceptibility χ and exchange relaxation damping σ on the domain-wall motion, we use the remainder of this section for analytical studies. We start from the constant saturation magnetization of a one-dimensional domain-wall model, such as the 1D head-to-head wall [43]. The static 1D domain-wall profile can be expressed as

$$m_x = -\tanh\left(\frac{x-q}{\Delta}\right), \quad m_t = \text{sech}\left(\frac{x-q}{\Delta}\right), \quad (31)$$

where m_t is the perpendicular component of the unit magnetization vector, Δ is the wall width parameter, and q is the position of the domain-wall center.

We consider the case in which the system is characterized by two anisotropies, easy uniaxial anisotropy K , and hard-plane anisotropy K_{\perp} , which originate from demagnetization. The aim is to analyze the impact of the longitudinal magnetic susceptibility under the 1D domain-wall model; the demagnetization energy density can be written as

$$E_{\text{an}} = -\frac{K}{M_e^2} M_x^2 + \frac{K_{\perp}}{M_e^2} M_z^2, \quad (32)$$

where $K = (1/2)(N_y - N_x)\mu_0 M_e^2$ and $K_{\perp} = (1/2)(N_z - N_y)\mu_0 M_e^2$. In the limit case $\chi \rightarrow 0$, the effective anisotropy energy density E_{an} can be rewritten as

$$E'_{\text{an}} = K \sin^2 \theta (1 + \kappa \sin^2 \varphi), \quad (33)$$

where $\mathbf{m} = (\cos \theta, \sin \theta \cos \varphi, \sin \theta \sin \varphi)$ is used and $\kappa = K_{\perp}/K$ is the ratio between hard-plane anisotropy strength and easy uniaxial anisotropy strength.

The dynamics of the domain wall with a 1D profile can be described using three parameters [44]: the domain-wall width Δ , the domain-wall position q , and the domain-wall tilt angle ϕ . In this domain-wall model, one can assume that $\varphi(x, t) = \phi(t)$ is only a function of time. Thus, the magnetization profile for the head-to-head domain wall is given by

$$\theta(x, t) = 2 \tan^{-1} \exp\left(\frac{x-q(t)}{\Delta(t)}\right), \quad \varphi(x, t) = \phi(t). \quad (34)$$

Using the magnetization unit vector to calculate the exchange energy is a good approximation for the case $\chi \ll 1$; thus, the total energy density can be rewritten as

$$E_{\text{tot}} = \frac{\mu_0}{8\chi} \frac{(M^2 - M_e^2)^2}{M_e^2} + M^2 w_{\mu}(\mathbf{m}), \quad (35)$$

where

$$w_{\mu}(\mathbf{m}) = \frac{A}{M_e^2} (\nabla \mathbf{m})^2 - \frac{K}{M_e^2} m_x^2 + \frac{K_{\perp}}{M_e^2} m_z^2. \quad (36)$$

Within the 1D domain-wall profile, H_m , the longitudinal component of the effective field, is obtained:

$$H_m = \mathbf{m} \cdot \mathbf{H}_{\text{eff}} = \frac{M}{2\chi M_e^2} (M_e^2 - M^2) - 2MP \sin^2 \theta, \quad (37)$$

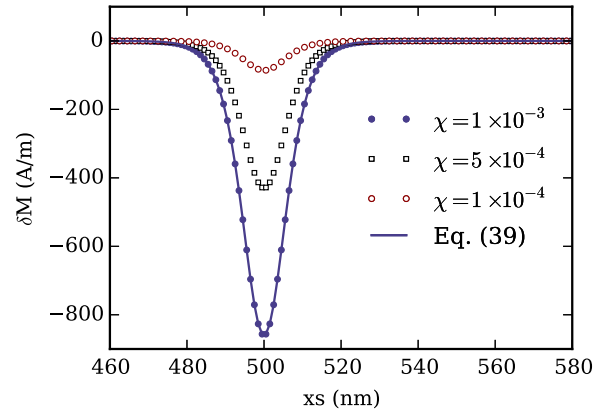


FIG. 5. (Color online) Simulation results of the magnetization length difference δM for a 1D domain wall located at $x = 500$ nm with $M_e = 8.6 \times 10^5$ A/m and $A = 1.3 \times 10^{-11}$ J/m. The demagnetization factors are selected to be $N_x = 0$ and $N_y = N_z = 0.5$.

where P is defined as

$$P = \frac{1}{\mu_0 M_e^2} \left[\frac{A}{\Delta^2} + K(1 + \kappa \sin^2 \phi) \right]. \quad (38)$$

As we can see, P is a function of the tilt angle ϕ and the domain-wall width Δ . At the static state, H_m should equal zero, i.e., $dM/dt = 0$, which gives

$$M^2 = (1 - 4\chi P \sin^2 \theta) M_e^2. \quad (39)$$

Equation (39) shows that the difference between magnetization length M and M_e reaches its maximum at the center of the domain wall due to the effect of the exchange field, which also peaks in the center of the domain wall. According to Eq. (39), we can estimate that the magnetization length difference is $\delta M \approx -2\chi P \sin^2 \theta$ for the $\chi \ll 1$ case. Figure 5 shows the magnetization length differences of a 1D domain wall for various χ ; it can be seen that this approximation for δM agrees very well with the simulation results.

In the dynamic case, H_m is not equal to zero. If we wrote Eq. (37) as $H_m = FM$, we would find that the nontrivial term that contributes to H_m is

$$F = \frac{1}{2\chi} (1 - M^2/M_e^2) - 2P \sin^2 \theta. \quad (40)$$

As an approximation for H_m , we expect $dF/dt = 0$ [45], which gives

$$H_m = \frac{4P}{\Delta} \frac{\chi}{\alpha} \frac{\dot{q}}{\gamma} m_t^2 m_x. \quad (41)$$

where we have used $\partial M/\partial t \approx \lambda_r H_m$. In addition, we have ignored the terms containing dP/dt , which is valid for a steady domain-wall motion. We employ the Lagrangian equation combined with dissipation function \mathcal{F} to compute the domain-wall dynamics [27]. The Lagrange equations are

$$\frac{\partial \mathcal{L}}{\partial X} - \frac{d}{dt} \left(\frac{\partial \mathcal{L}}{\partial \dot{X}} \right) + \frac{\partial \mathcal{F}}{\partial \dot{X}} = 0, \quad (42)$$

where X refers to q , ϕ , and Δ . The dissipation function is defined by $\mathcal{F} = \int F dx$, where

$$F = \frac{1}{2} \mu_0 M_e \gamma [\alpha \mathbf{H}_{\text{eff}}^2 + \sigma (\nabla \mathbf{H}_{\text{eff}})^2] \quad (43)$$

is the dissipation density function.

A. Parallel relaxation

We neglect the exchange-damping term with assumption that $\sigma \ll \alpha \Delta^2$ and arrive at

$$F = \frac{1}{2} \alpha \mu_0 M_e \gamma \mathbf{H}_{\text{eff}}^2 = \frac{1}{2} \alpha \mu_0 M_e \gamma (\mathbf{H}_{\perp}^2 + \mathbf{H}_m^2), \quad (44)$$

where \mathbf{H}_{\perp} and \mathbf{H}_m are the perpendicular and parallel components of the effective field. If we also assume that $\alpha \sim \chi \ll 1$, \mathbf{H}_{\perp}^2 can be approximated by Eq. (11),

$$\mathbf{H}_{\perp}^2 = \frac{1}{\gamma^2} \dot{\mathbf{m}}^2 = \frac{1}{\gamma^2} (\dot{\theta}^2 + \sin^2 \theta \dot{\phi}^2). \quad (45)$$

Substituting Eqs. (41) and (45) into Eq. (44) and integrating over space, we obtain

$$\mathcal{F} = \frac{\alpha \mu_0 M_e}{\gamma} \left[\dot{\phi}^2 \Delta + \frac{\dot{q}^2}{\Delta} (1 + Q) \right], \quad (46)$$

where we have ignored the $\dot{\Delta}$ term. This term leads to the optimal domain-wall width [27]:

$$\Delta = \sqrt{A/(K + K_{\perp} \sin^2 \phi)}, \quad (47)$$

and for $\kappa = 0$ the optimal domain-wall width reduces to $\Delta_0 = \sqrt{A/K}$. In what follows, the domain-wall-width parameter $\Delta(t)$ is approximated by the optimal wall width. The parameter P is then given by

$$P = \frac{2K(1 + \kappa \sin^2 \phi)}{\mu_0 M_e^2} = \frac{2}{\mu_0 M_e^2} \frac{A}{\Delta^2}, \quad (48)$$

and it is straightforward to find its minimum $P_0 = 2K/(\mu_0 M_e^2)$, which corresponds to $\Delta = \Delta_0$.

The introduced parameter Q in Eq. (46) is given by $Q = (32/15)P^2(\chi/\alpha)^2$, and its value is determined by the ratio of χ and α , which could be ~ 1 , although we assume $\chi \sim \alpha \ll 1$. Following the treatment of Ref. [27], the integrated Lagrangian action \mathcal{L} is given by

$$\begin{aligned} \mathcal{L} &= \int \left(E_{\text{tot}} + \frac{\mu_0 M_e}{\gamma} \dot{\phi} \cos \theta \right) dx \\ &= \frac{2A}{\Delta} + 2\Delta K(1 + \kappa \sin^2 \phi)(1 - V) \\ &\quad - 2\mu_0 M_e H_a q + \frac{2\mu_0 M_e}{\gamma} \dot{\phi} q, \end{aligned} \quad (49)$$

where $\mu_0 M_e \dot{\phi} \cos \theta / \gamma$ is the Berry phase term [46] and $V = 8\chi P/3$ is a result of the varying magnetization that introduced a pinning potential. However, the potential is fairly small and therefore is negligible since $V \ll Q$. By substituting Eqs. (49) and (44) into Eq. (42),

$$\begin{aligned} \dot{\phi} + \alpha \frac{\dot{q}}{\Delta} (1 + Q) &= \gamma H_a, \\ \frac{\dot{q}}{\Delta} - \alpha \dot{\phi} &= \gamma \frac{H_k}{2} \sin 2\phi, \end{aligned} \quad (50)$$

where $H_k = 2K_{\perp}/(\mu_0 M_e)$. The domain-wall dynamics is governed by Eq. (50); by eliminating \dot{q} we obtain an equation about $\dot{\phi}$,

$$\dot{\phi} = \frac{\gamma}{1 + \alpha^2(1 + Q)} [H_a - H_w(1 + Q) \sin 2\phi], \quad (51)$$

where $H_w = \alpha H_k/2$ is the Walker breakdown field. From Eq. (51) we can find that the critical value of ϕ is approximately equal to $\pi/4$ if $Q \ll 1$, which leads to the maximum value of P being $P_1 = 2K(1 + \kappa/2)/(\mu_0 M_e^2)$. There exists an equilibrium state ϕ^* such that $\dot{\phi} = 0$ if $H_a < H_w(1 + Q)$,

$$\sin(2\phi^*) = h \equiv \frac{H_a}{H_w(1 + Q)}, \quad (52)$$

which means the Walker breakdown field H'_w for the $\chi > 0$ case is increased to $H_w(1 + \max\{Q\})$, i.e.,

$$H'_w = H_w \left[1 + \frac{32}{15} P_1^2 \left(\frac{\chi}{\alpha} \right)^2 \right], \quad (53)$$

where P_1 is the maximum value of P . For this steady-state wall motion, the domain-wall velocity is

$$\dot{q} = \frac{\gamma H_a}{\alpha} \frac{\Delta^*}{1 + Q(\Delta^*)}, \quad (54)$$

where

$$\Delta^* = \Delta_0 / \sqrt{1 + \frac{\kappa}{2}(1 - \sqrt{1 - h^2})}. \quad (55)$$

Therefore, $\Delta^* \rightarrow \Delta_0$ in the limit case $H_a \rightarrow 0$, and the domain-wall mobility μ is given by

$$\mu = \frac{\gamma \Delta}{\alpha} \left[1 + \frac{32}{15} P_0^2 \left(\frac{\chi}{\alpha} \right)^2 \right]^{-1}, \quad (56)$$

where P_0 is the minimum value of P . In Fig. 4 the corresponding Walker breakdown fields are plotted as vertical dashed lines, which gives a good approximation of the $\chi = 5 \times 10^{-4}$ and $\chi = 1 \times 10^{-4}$ cases. The simulation results show that the Walker breakdown field H_w could be changed significantly if the longitudinal susceptibility is comparable to the damping constant.

B. Nonlocal damping

In this part we consider the domain-wall motion influenced by exchange damping for the case in which $\chi \rightarrow 0$. The dissipation density function (43) thus becomes

$$F = \frac{1}{2} \mu_0 M_e \gamma [\alpha \mathbf{H}_{\perp}^2 + \sigma (\nabla H_{\theta})^2 + \sigma (\nabla H_{\phi})^2], \quad (57)$$

where H_{θ} and H_{ϕ} are the two components of the effective field and \mathbf{H}_{\perp} is computed using Eq. (45). After performing the calculation we obtain

$$\mathcal{F} = \frac{\mu_0 M_e}{\gamma} \left[\dot{\phi}^2 \left(\alpha \Delta + \frac{1}{3} \frac{\sigma}{\Delta} \right) + \frac{\dot{q}^2}{\Delta} \left(\alpha + \frac{1}{3} \frac{\sigma}{\Delta^2} \right) \right]. \quad (58)$$

We take the same Lagrangian action (49) for $\chi = 0$ and arrive at

$$\begin{aligned} \dot{\phi} + \left(\alpha + \frac{\sigma}{3\Delta^2} \right) \frac{\dot{q}}{\Delta} &= \gamma H_a, \\ \frac{\dot{q}}{\Delta} - \left(\alpha + \frac{\sigma}{3\Delta^2} \right) \dot{\phi} &= \gamma \frac{H_k}{2} \sin 2\phi. \end{aligned} \quad (59)$$

Similarly, the corresponding Walker breakdown field changes to

$$H'_w = \frac{1}{2} H_k \left(\alpha + \frac{1}{3} \frac{\sigma}{\Delta_1^2} \right), \quad (60)$$

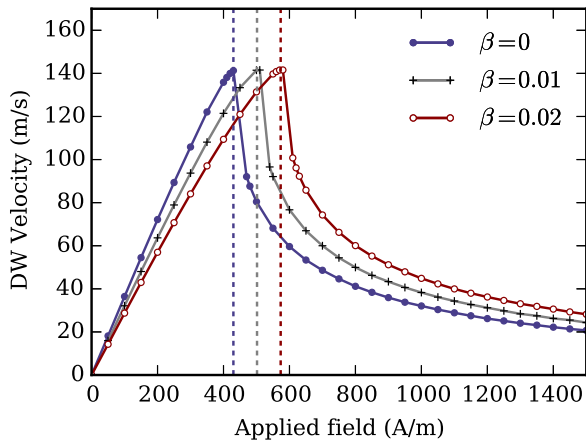


FIG. 6. (Color online) Simulation results of domain-wall velocities for the limit case that $\chi \rightarrow 0$ with various exchange dampings. The parameters used are $\alpha = 0.005$, $N_y = 0.4$, and $N_z = 0.6$. The vertical dashed lines are the breakdown fields computed with Eq. (60).

where $\Delta_1 = \Delta_0 \sqrt{1/(1 + \kappa/2)}$. The domain-wall mobility is given by

$$\frac{1}{\mu} = \frac{1}{\gamma \Delta_0} \left(\alpha + \frac{1}{3} \frac{\sigma}{\Delta_0^2} \right). \quad (61)$$

As we can see, the nonlocal damping term σ influences the domain-wall motion as well, and we can establish that $\sigma/\Delta^2 = \beta(1 + \kappa/2)K/(\mu_0 M_e^2) \propto \beta$. Therefore, for the scenarios in which $K \sim \mu_0 M_e^2$, the contributions from the Gilbert and nonlocal damping are of the order of magnitude of both the domain-wall mobility and Walker breakdown field.

Figure 6 shows the domain-wall velocities for domain-wall motion driven by external fields in the limiting case of $\chi \rightarrow 0$. The simulation results are based on a one-dimensional mesh with a length of 10 000 nm, discretized with a cell size of 2 nm. The damping α is set to 0.005, and the demagnetizing factors are chosen to be $N_x = 0$, $N_y = 0.4$, and $N_z = 0.6$. As predicted by Eq. (60), the nonlocal damping β leads to an increment of the Walker breakdown field, and Eq. (60) fits the simulation results very well.

VI. SUMMARY

We explain the exchange damping in the LLBar equation as nonlocal damping by linking it to the spin current pumping, and therefore, the LLBar (17) can be considered a phenomenological equation to describe the nonlocal damping. In the presence of nonlocal damping, the lifetime and propagation length of short-wavelength magnons could be much shorter than those given by the LLG equation. Our simulation results show that the spin-wave amplitude decays much faster in the presence of nonlocal damping when spin waves propagate along a single rod. The analytical result shows that there is extra nonlinear dependence scaling with k^2 between λk (the product of spin-wave-decay constant λ and wave vector k) and frequency ω due to the nonlocal damping. Using the micromagnetic simulation based on the LLBar equation, we show that the difference between magnetization length M and M_e reaches its maximum

at the center of the domain wall. For the cases in which $\chi \sim \alpha$, where χ is the longitudinal magnetic susceptibility and α is the Gilbert damping, the Walker breakdown field will increase significantly. By using a 1D domain-wall model, we also show that both the domain-wall mobility and the Walker breakdown field are strongly influenced by the nonlocal damping as well.

ACKNOWLEDGMENTS

We acknowledge the financial support from EPSRC's DTC Grant No. EP/G03690X/1. W.W. thanks the China Scholarship Council for financial assistance. The research leading to these results has received funding from the European Community's Seventh Framework Programme (FP7/2007-2013) under Grant Agreement No. 247556 (NoWaPhen) and from the European Union's Horizon 2020 research and innovation program under Marie Skłodowska-Curie Grant Agreement No. 644348 (MagIC).

APPENDIX A: DERIVATION OF EQUATION (16)

We split the perpendicular spin current $\mathbf{j}_{\perp,i}$ into two components,

$$\mathbf{j}_{\perp,i} = \mathbf{j}_i^a + \mathbf{j}_i^b, \quad (A1)$$

where we write λ_e/γ as $\tilde{\sigma}$,

$$\mathbf{j}_i^a = -\tilde{\sigma}(\partial_i \mathbf{m} \times \partial_t \mathbf{m}), \quad (A2)$$

$$\mathbf{j}_i^b = -\tilde{\sigma}(\mathbf{m} \times \partial_t \partial_i \mathbf{m}). \quad (A3)$$

The torque $\boldsymbol{\tau}_a$ generated by spin current \mathbf{j}_i^a is given by $\boldsymbol{\tau}_a = (\partial_i \mathbf{j}_i^a)_{\perp}$, i.e.,

$$\boldsymbol{\tau}_a = \tilde{\sigma} \mathbf{m} \times [\partial_t \mathbf{m} \times (\partial_t \mathbf{m} \times \partial_t \mathbf{m})], \quad (A4)$$

where we have used the identities $\mathbf{m} \cdot \partial_i \partial_t \mathbf{m} = -\partial_t \mathbf{m} \cdot \partial_i \mathbf{m}$ and $\mathbf{m} \cdot \partial_t \partial_i \mathbf{m} = -\partial_t \mathbf{m} \cdot \partial_i \mathbf{m}$. Meanwhile, the corresponding torque $\boldsymbol{\tau}_b$ can be computed by $\boldsymbol{\tau}_b = (\partial_i \mathbf{j}_i^b)_{\perp}$, which gives

$$\boldsymbol{\tau}_b = \boldsymbol{\tau}_a - \tilde{\sigma}(\partial_i \mathbf{m} \cdot \partial_i \mathbf{m}) \mathbf{m} \times \partial_t \mathbf{m} - \tilde{\sigma} \mathbf{m} \times \nabla^2 \partial_t \mathbf{m}. \quad (A5)$$

Note that $\boldsymbol{\tau}_a = \tilde{\sigma} \partial_t \mathbf{m} [(\partial_t \mathbf{m} \times \partial_t \mathbf{m}) \cdot \mathbf{m}]$ can be changed into the tensor form,

$$\boldsymbol{\tau}_a = \mathbf{m} \times (\mathcal{D}^0 \cdot \partial_t \mathbf{m}), \quad (A6)$$

where

$$\mathcal{D}_{\alpha\beta}^0 = \tilde{\sigma}(\mathbf{m} \times \partial_i \mathbf{m})_{\alpha}(\mathbf{m} \times \partial_i \mathbf{m})_{\beta}. \quad (A7)$$

Therefore, we obtain, for $\boldsymbol{\tau}_a + \boldsymbol{\tau}_b$,

$$\boldsymbol{\tau}_a + \boldsymbol{\tau}_b = \mathbf{m} \times (\mathcal{D} \cdot \partial_t \mathbf{m}) - \tilde{\sigma} \mathbf{m} \times \nabla^2 \partial_t \mathbf{m}, \quad (A8)$$

where \mathcal{D} is a 3×3 tensor,

$$\mathcal{D}_{\alpha\beta} = 2\tilde{\sigma}(\mathbf{m} \times \partial_i \mathbf{m})_{\alpha}(\mathbf{m} \times \partial_i \mathbf{m})_{\beta} - \tilde{\sigma}(\partial_i \mathbf{m} \cdot \partial_i \mathbf{m})\delta_{\alpha\beta}. \quad (A9)$$

APPENDIX B: DERIVATION OF EQUATION (27)

We introduce a new variable \mathbf{s} to represent the second term in (23), i.e., $\mathbf{s} = \mathbf{m}_0 e^{i(\tilde{k}x - \omega t)}$, so we have

$$\mathbf{m} = \mathbf{e}_x + \mathbf{s}, \quad (\text{B1})$$

$$\frac{d\mathbf{m}}{dt} = -i\omega\mathbf{s}, \quad (\text{B2})$$

$$\mathbf{H}_{\text{eff}} = H_s(1 + s'_x)\mathbf{e}_x - D\tilde{k}^2\mathbf{s}, \quad (\text{B3})$$

where $s'_x \approx (1/2)(s_x^2 - s^2)$. Considering the fact $|\mathbf{s}| \ll 1$ and neglecting the high-order term s^2 , one obtains $\mathbf{H}_{\text{eff}}^{\perp} = -(H_s + D\tilde{k}^2)\mathbf{s}$ and thus

$$\mathbf{H}_{\text{eff}}^b = c\mathbf{e}_x + d\mathbf{s}, \quad (\text{B4})$$

where

$$c = \alpha H_s(1 + s'_x), \quad (\text{B5})$$

$$d = -\beta G\tilde{k}^2(D\tilde{k}^2 + H_s) - \alpha D\tilde{k}^2. \quad (\text{B6})$$

Substituting the above equations into (17), we have

$$\frac{i\omega}{\gamma} \begin{bmatrix} s_x \\ s_y \\ s_z \end{bmatrix} = f \begin{bmatrix} 0 \\ s_z \\ -s_y \end{bmatrix} + (c-d) \begin{bmatrix} -(s_y^2 + s_z^2) \\ (1+s_x)s_y \\ (1+s_x)s_z \end{bmatrix}, \quad (\text{B7})$$

where $f = H_s(1 + s'_x) + D\tilde{k}^2$. Neglecting high-order terms such as s_x^2 and $s_x s_y$, we obtain

$$\begin{bmatrix} \gamma(\alpha H_s - d) - i\omega & \tilde{w}_0 \\ -\tilde{w}_0 & \gamma(\alpha H_s - d) - i\omega \end{bmatrix} \begin{bmatrix} s_y \\ s_z \end{bmatrix} = \begin{bmatrix} 0 \\ 0 \end{bmatrix}. \quad (\text{B8})$$

Therefore, Eq. (27) can be obtained by setting the determinant of the matrix in (B8) to zero.

-
- [1] L. Landau and E. Lifshitz, *Phys. Z. Sowjetunion* **8**, 153 (1935).
[2] A. I. Akhiezer, V. G. Bar'yakhtar, and S. V. Peletminskii, *Spin Waves* (North-Holland, Amsterdam, 1968).
[3] M. Donahue and D. Porter, OOMMF, version 1.0, NIST, Gaithersburg, MD, 1999; <http://math.nist.gov/oommf/>.
[4] W. Scholz, J. Fidler, T. Schrefl, D. Suess, R. Dittrich, H. Forster, and V. Tsiantos, *Comput. Mater. Sci.* **28**, 366 (2003).
[5] T. Fischbacher, M. Franchin, G. Bordignon, and H. Fangohr, *IEEE Trans. Magn.* **43**, 2896 (2007).
[6] D. V. Berkov and N. L. Gorn, *J. Phys. D: Appl. Phys.* **41**, 164013 (2008).
[7] A. Vansteenkiste, J. Leliaert, M. Dvornik, M. Helsen, F. Garcia-Sanchez, and B. Van Waeyenberge, *AIP Adv.* **4**, 107133 (2014).
[8] T. Gilbert, *IEEE Trans. Magn.* **40**, 3443 (2004).
[9] J. L. García-Palacios and F. J. Lázaro, *Phys. Rev. B* **58**, 14937 (1998).
[10] Y. Shu, M. Lin, and K. Wu, *Mech. Mater.* **36**, 975 (2004).
[11] S. Zhang and Z. Li, *Phys. Rev. Lett.* **93**, 127204 (2004).
[12] A. Thiaville, Y. Nakatani, J. Miltat, and Y. Suzuki, *Europhys. Lett.* **69**, 990 (2005).
[13] K. M. Lebecki, M. J. Donahue, and M. W. Gutowski, *J. Phys. D: Appl. Phys.* **41**, 175005 (2008).
[14] W. Wang, C. Mu, B. Zhang, Q. Liu, J. Wang, and D. Xue, *Comput. Mater. Sci.* **49**, 84 (2010).
[15] B. Krueger and G. Selke, *IEEE Trans. Magn.* **49**, 4749 (2013).
[16] A. Kirilyuk, A. V. Kimel, and T. Rasing, *Rev. Mod. Phys.* **82**, 2731 (2010).
[17] Y. Au, M. Dvornik, T. Davison, E. Ahmad, P. S. Keatley, A. Vansteenkiste, B. Van Waeyenberge, and V. V. Kruglyak, *Phys. Rev. Lett.* **110**, 097201 (2013).
[18] B. D. Terris and T. Thomson, *J. Phys. D: Appl. Phys.* **38**, R199 (2005).
[19] V. V. Kruglyak, S. O. Demokritov, and D. Grundler, *J. Phys. D: Appl. Phys.* **43**, 264001 (2010).
[20] V. G. Baryakhtar, in *Frontiers in Magnetism of Reduced Dimension Systems*, edited by V. G. Baryakhtar, P. E. Wigen, and N. A. Lesnik, NATO ASI Series, Vol. 49 (Springer, Netherlands, 1998), pp. 63–94.
[21] V. G. Bar'yakhtar, B. A. Ivanov, T. K. Soboleva, and A. L. Sukstanskii, *Zh. Eksp. Teor. Fiz* **91**, 1454 (1986) [*Sov. Phys. JETP* **64**, 857 (1986)].
[22] V. G. Baryakhtar and A. G. Danilevich, *Low Temp. Phys.* **39**, 993 (2013).
[23] S. Zhang and S. S.-L. Zhang, *Phys. Rev. Lett.* **102**, 086601 (2009).
[24] L. De Angeli, D. Steiauf, R. Singer, I. Köberle, F. Dietermann, and M. Fähnle, *Phys. Rev. B* **79**, 052406 (2009).
[25] M. Dvornik, A. Vansteenkiste, and B. Van Waeyenberge, *Phys. Rev. B* **88**, 054427 (2013).
[26] I. A. Yastremsky, P. M. Oppeneer, and B. A. Ivanov, *Phys. Rev. B* **90**, 024409 (2014).
[27] B. Hillebrands and A. Thiaville, *Spin Dynamics in Confined Magnetic Structures III* (Springer, New York, 2006).
[28] T. Weindler, H. G. Bauer, R. Islinger, B. Boehm, J.-Y. Chauleau, and C. H. Back, *Phys. Rev. Lett.* **113**, 237204 (2014).
[29] V. G. Bar'yakhtar, *Zh. Eksp. Teor. Fiz* **87**, 1501 (1984) [*Sov. Phys. JETP* **60**, 863 (1984)].
[30] U. Atxitia and O. Chubykalo-Fesenko, *Phys. Rev. B* **84**, 144414 (2011).
[31] Y. Tserkovnyak, E. M. Hankiewicz, and G. Vignale, *Phys. Rev. B* **79**, 094415 (2009).
[32] M. Fähnle and S. Zhang, *J. Magn. Magn. Mater.* **326**, 232 (2013).
[33] E. M. Hankiewicz, G. Vignale, and Y. Tserkovnyak, *Phys. Rev. B* **78**, 020404 (2008).
[34] M. C. Hickey and J. S. Moodera, *Phys. Rev. Lett.* **102**, 137601 (2009).
[35] H. T. Nembach, J. M. Shaw, C. T. Boone, and T. J. Silva, *Phys. Rev. Lett.* **110**, 117201 (2013).
[36] D.-S. Han, S.-K. Kim, J.-Y. Lee, S. J. Hermsdoerfer, H. Schultheiss, B. Leven, and B. Hillebrands, *Appl. Phys. Lett.* **94**, 112502 (2009).
[37] S.-M. Seo, K.-J. Lee, H. Yang, and T. Ono, *Phys. Rev. Lett.* **102**, 147202 (2009).
[38] V. G. Baryakhtar, *Low Temp. Phys.* **40**, 626 (2014).
[39] C. Kittel, *Phys. Rev.* **110**, 1295 (1958).
[40] D. Stancil and A. Prabhakar, *Spin Waves: Theory and Applications* (Springer, Berlin, 2009).

- [41] M. Dvornik, Y. Au, and V. V. Kruglyak, *Top. Appl. Phys.*, **125**, 101 (2013).
- [42] R. Liu, J. Wang, Q. Liu, H. Wang, and C. Jiang, *J. Appl. Phys.* **103**, 013910 (2008).
- [43] Y. Nakatani, A. Thiaville, and J. Miltat, *J. Magn. Magn. Mater.* **290-291**, 750 (2005).
- [44] L. O'Brien, E. R. Lewis, A. Fernández-Pacheco, D. Petit, R. P. Cowburn, J. Sampaio, and D. E. Read, *Phys. Rev. Lett.* **108**, 187202 (2012).
- [45] V. L. Sobolev, S. C. Chen, and H. L. Huang, *J. Magn. Magn. Mater.* **172**, 83 (1997).
- [46] J. Shibata, G. Tatara, and H. Kohno, *J. Phys. D: Appl. Phys.* **44**, 384004 (2011).